Examination of the Bouchet–Morton Complementary Relationship Using a Mesoscale Climate Model and Observations under a Progressive Irrigation Scenario

MUTLU OZDOGAN

NASA GSFC, Greenbelt, Maryland

GUIDO D. SALVUCCI AND BRUCE T. ANDERSON

Department of Geography, Boston University, Boston, Massachusetts

(Manuscript received 10 November 2004, in final form 29 April 2005)

ABSTRACT

The complementary relationship between actual and potential evaporation over southeastern Turkey was examined using a mesoscale climate model and field data. Model simulations of both actual and potential evaporation produce realistic temporal patterns in comparison to those estimated from field data; as evaporation from the surface increases with increasing irrigation, potential evaporation decreases. This is in accordance with the Bouchet–Morton complementary relationship and suggests that actual evapotranspiration can be readily computed from routine meteorological observations. The driving mechanisms behind irrigation-related changes in actual and potential evaporation include reduced wind velocities, increased atmospheric stability, and depressed humidity deficits. The relative role of each in preserving the complementary relation is assessed by fitting a potential evaporation model to pan evaporation data. The importance of reduced wind velocity in maintaining complementarity was unexpected, and thus examined further using a set of perturbation simulation experiments with changing roughness parameters (reflecting growing cotton crops), changing moisture conditions (reflecting irrigation), and both. Three potential causes of wind velocity reduction associated with irrigation may be increased surface roughness, decreased thermal convection that influences momentum transfer, and the development of anomalous high pressure that counteracts the background wind field. All three are evident in the mesoscale model results, but the primary cause is the pressure-induced local wind system. The apparent necessity of capturing mesoscale dynamical feedbacks in maintaining complementarity between potential and actual evaporation suggests that a theory more complicated than current descriptions (which are based on feedbacks between actual evaporation and temperature and/or humidity gradients) is required to explain the complementary relationship.

1. Introduction

It is widely accepted that regional evapotranspiration from land surfaces is difficult to estimate and remains one of the most poorly understood components of the hydrologic cycle (Entekhabi et al. 1999). In part, this difficulty stems from lack of reliable data on soil moisture, especially in highly variable surfaces. Additionally, most routine methods to estimate evapotranspiration require hard-to-obtain parameters such as turbulent transfer coefficients and stomatal conductances. Thus, evaporation estimation methods that avoid the use of rarely available soil moisture data and are simple enough to be used with routinely available meteorological data are highly desirable.

One such method is the complementary relationship (hereafter CR) first proposed by Bouchet (1963) and further developed by Morton (1965). Originally based entirely on heuristic arguments, the theory of complementarity has found wide support in the literature both through comparison to other methods that estimate evapotranspiration (Parlange and Katul 1992; Qualls and Gultekin 1997) and through analysis based on meteorological observations and/or modeling results (Hobbins et al. 2001; Sugita et al. 2001; Ozdogan and Salvucci 2004; Hobbins et al. 2004). Other recent research is focused on finding a more physical foundation for the CR (e.g., Kim and Entekhabi 1997; Szilagyi 2001).

Corresponding author address: Mutlu Ozdogan, NASA GSFC, Code 614.3, Greenbelt, MD 20771.
E-mail: ozdogan@hsb.gsfc.nasa.gov

The purpose of the study presented herein is to investigate the validity of the CR in southeastern Turkey with the help of a mesoscale climate model as well as with meteorological data. The CR was evaluated within the climate model by performing 10-day midsummer simulations to determine the changes in hydrologic fluxes under a progressive irrigation development scenario. The model, which forecasts regional meteorological and surface conditions, implicitly captures the feedbacks between potential and actual evaporation by updating the temperature and moisture fields, both at the surface and in the overlying atmosphere, which subsequently moderates the interaction between the two. This makes the model a reasonable forecasting tool for this region and a reasonable tool for supporting or contradicting the theory of complementarity. The CR was further analyzed by estimating the terms of the Penman equation [including the Monin–Obukhov (1954) (M–O) stability parameters] that was calibrated to measured pan evaporation. Because M–O characterization requires specification of the sensible heat flux (H), a simple land surface energy balance was computed to estimate H in conjunction with the potential evaporation equation.

By combining the results from the climate model and meteorological data, it was possible to (i) test the CR purely in the mesoscale model; (ii) compare potential evaporation estimates between the climate model, pan evaporation data, and calibrated potential evaporation equations; (iii) estimate the M–O scaling variables (which include instability) for comparing environmental variables such as wind speed and humidity between the climate model and observations; (iv) have a calibrated potential evaporation equation with which sensitivity analyses could be performed to explore the relative importance of variables like humidity and wind speed for maintaining complementarity; and (v) explore the larger-scale, dynamical feedbacks controlling the wind speed decreases reported in Ozdogan and Salvucci (2004). As an example of a unique long-running experiment, the data collected throughout the extensive irrigation development projects in southeastern Turkey provide an opportunity to perform and evaluate each of these tasks.

2. The complementary relationship

The CR states that under constant energy input and away from sharp discontinuities there exists a complementary feedback mechanism between actual (E_a) and potential (E_p) evapotranspiration that causes changes in each to be complementary, that is, a unit decrease in E_a causes a unit increase in E_p. Here, E_p is defined as the evapotranspiration given by the Penman equation using meteorological variables under prevailing atmospheric conditions. In contrast, a sufficiently moist uniform surface evapotranspiring at the potential rate under steady-state conditions would be defined as equilibrium, or wet-environment, evapotranspiration (E_w) [after Morton (1965) and Brutsaert and Stricker (1979)]. Bouchet (1963) hypothesized that under conditions of minimal advection, when E_a, due to limited water availability, falls below its potential rate (E_w), a certain amount of energy (Q) would become available:

$$\lambda E_w - \lambda E_a = Q. \tag{1}$$

This excess energy not used for evapotranspiration would then warm the atmosphere. Increased air temperature due to this warming and decreased humidity due to reduced evapotranspiration would then lead to a "new" potential evapotranspiration (E_p) that is larger than E_w by the amount Q:

$$\lambda E_w + Q = \lambda E_p. \tag{2}$$

Combining Eqs. (1) and (2) lead to the complementary relationship (Fig. 1)

$$\lambda E_a = 2\lambda E_w - \lambda E_p. \tag{3}$$

If water availability at the surface is increased—for example, through irrigation—the reverse process occurs, and E_p decreases as E_a increases. Thus, potential evaporation measured over a region becomes both the result and cause of actual evaporation measured over the same region.

In evaluating the CR, E_p is commonly computed with the combination equation of Penman (1948) and E_w with the empirical equation of Priestley and Taylor

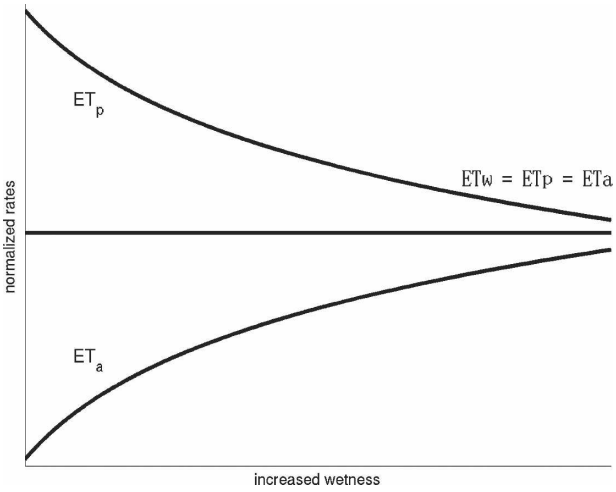

FIG. 1. Schematic representation of the CR, where ET_a is actual evapotranspiration, ET_p is potential evapotranspiration, and ET_w is wet-environment evapotranspiration. The x axis represents increasing wetness.

(1972) for conditions of minimal advection. In this research, the CR is evaluated by comparing model-simulated and observed E_p and E_a to those computed by the calibrated Penman equation.

3. Climate model description

The simulation of E_p and E_a under a progressive irrigation development scenario was performed using the National Centers for Environmental Prediction (NCEP) Regional Spectral Modeling (RSM) system (Juang and Kanamitsu 1994; Juang et al. 1997). The NCEP global to regional modeling system contains two components—a low-resolution Global Spectral Model (GSM) and a Regional Spectral Model with multiple nests (RSM1 and RSM2). The nesting method is a one-way, noninteractive procedure, designed to calculate regional responses (or adjustments) of the RSM to the large-scale background fields provided by the coarser-resolution GSM and RSM1, respectively (Juang and Kanamitsu 1994; Juang et al. 1997). The multinesting allows the model system to capture the finescale features such as changing surface conditions (e.g., enhanced irrigation) in the RSM, while still incorporating the development of large-scale synoptic features in the GSM. The resolution of the GSM is triangular-62 (T62, approximately 200 km); the resolutions for the RSM1 and RSM2 are chosen as 25 and 10 km, respectively, for the study region. A portion of the RSM2 domain over the Harran Plain is shown in Fig. 2.

Particularly important in this study is the Land Surface Model (LSM) though which the coupled transport of momentum, heat, and moisture across the soil and vegetation layers are computed. The LSM coupled to the RSM is an early version of the NOAH land surface scheme as described in Chen et al. (1996). The NOAH LSM is a one-dimensional model with explicit vegetation canopy, soil hydrology, and soil thermodynamics. It employs a homogeneous soil scheme (with two layers) and vegetation type where vegetation fraction (σ_f) is set at 0.7 for each grid. The model simulates soil moisture, soil temperature, skin temperature, canopy water contents, and the energy and water flux terms of the surface energy and water balance. The turbulent flux computations use expressions derived from Monin–Obukhov similarity theory. In particular, evaporation (E_a) is computed as the sum of three parts: bare soil evaporation, canopy re-evaporation, and transpiration, each bounded by the potential evaporation (E_p), which itself is calculated using a Penman-based energy balance approach supplemented by atmospheric stability corrections (Mahrt and Ek 1984). For further details, the reader is referred to Chen et al. (1996).

The planetary boundary layer (PBL) processes

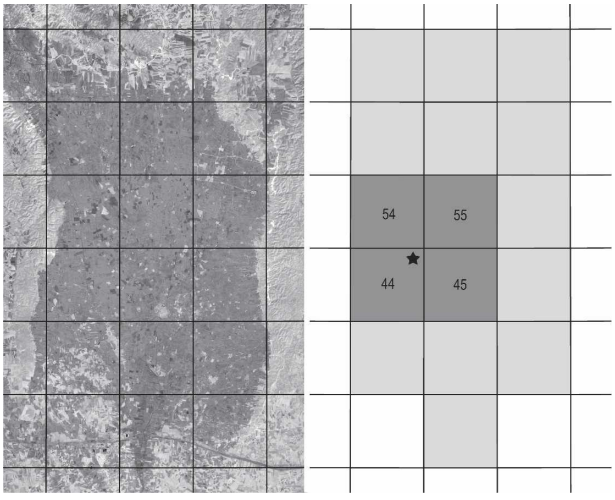

FIG. 2. Representation of irrigated fields within the Regional Spectral Model. The graphic on the left shows the irrigated Harran Plain as seen by the Landsat satellite. The dark gray colors indicate the presence of irrigated croplands. The graphic on the right shows grid box representation of the irrigated fields within the model. The location of the Koruklu meteorological station (black star) and grids 44, 45, 54, and 55 (darker gray) are shown for reference. Only a portion of the full modeling domain is shown. The bottom edge of each graphic is ~40 km.

(Hong and Pan 1996) are based on vertical diffusion in which the surface layer and PBL are coupled using a prescribed profile with similarity-based scale parameters. PBL height is computed iteratively by first computing the height without accounting for virtual temperature instability near the surface; from this estimate, calculations of vertical velocities can be obtained, which then allow estimation of the virtual temperature instability and subsequently modified boundary layer heights (Hong and Pan 1996). The diffusion parameters for momentum and mass (evaporation) are then determined from the boundary layer height using the prescribed profile shape.

As described in section 2, the CR arises from the feedback mechanisms within the PBL. One of the strengths of using a mesoscale climate model to evaluate CR is the relatively complete accounting of interactions between the surface and the PBL as well as between PBL and the free atmosphere. Thus, key physical processes such as radiative forcing (both surface and atmospheric) and stability of the atmosphere are continuously updated as a function of changing surface conditions (i.e., irrigation in these experiments) such that their effects on E_a and E_p are accounted for. This approach is in contrast with some earlier model-based evaluations of the CR using simple mixed-layer models (e.g., McNaughton and Spriggs 1989; Lhomme 1997).

4. Experimental design

For this study, we identified a small area of 100 grid elements (10 × 10 grids) within a large simulation domain configuration with a 10-km grid spacing centered over the Harran Plain, where the primary irrigation projects occurred in southeastern Turkey (see the subset of this domain in Fig. 2). One parameter we adjusted was the roughness length (Z_0). In the Harran Plain, fully developed irrigated crops (in July) represent rougher surfaces compared to nonirrigated fallow fields (in June). This change in roughness due to irrigation was estimated by comparing potential evaporation computed using a Penman-based approach (described in detail in the next section) and independent pan evaporation data. The results of this comparison are given in Fig. 3 where June, July, and August standardized root-mean-square error (rmse_S) values (Willmott 1982) between potential and pan evaporation data are plotted for a range of roughness lengths. The best-fit roughness for August (which represents fully irrigated crop development) is roughly 1.9 times the roughness length for June (which represents irrigated crop bud-break equivalent to nonirrigated roughness conditions).

It is interesting to note that the pan evaporation changes with (responds to) changes in roughness length over time. A common theme revisited many times in this paper, and central to the CR, is to measure the environment by its effect on pan evaporation. Based on the estimated fractional change in roughness lengths between August and June, for each irrigated grid, Z_0 in the model was increased to approximately twice the average default value of 0.5 m. While this new Z_0 value may appear to be too large to represent cotton (the primary irrigated crop in the Harran Plain with a maximum height of 1 m), in the context of the model, it represents the roughness length associated with topography and other surface elements within a 10-km lateral resolution as well as the vegetation; the doubling of the model values in the irrigated runs in turn preserves the observed relative change in Z_0 for mature crop conditions (i.e., twice as much). Our RSM simulations consisted of 16 progressive irrigation scenarios corresponding to two decades of irrigation expansion in southeastern Turkey. The location of irrigated areas for each year was based on remote sensing estimates between 1980 and 2000 as described in detail by Ozdogan et al. (2006) (see Fig. 2). However, since none of the irrigated areas was large enough to correspond to an entire model grid box (100 km^2), irrigation was represented by a total of 16 simulations (years), rather than 20. In other words, due to the regularized nature of simulation (i.e., surface is represented by grids rather than as a continuum) it took only 16 simulation years to represent the changes in irrigated areas that occurred in 20 yr in the real world.

For each 10-day simulation period (1–10 July), we used identical lateral boundary conditions (corresponding to July 2000) to isolate the effects of irrigation. We chose July 2000 not only because it represents the peak irrigation and mature crop period in the region, but also because the observed atmospheric conditions from the NCEP reanalysis data (Kalnay et al. 1996) indicated a relatively event free period (i.e., characterized by weak synoptic forcing).

For each irrigation year a grid designated as irrigated from remote sensing was saturated by artificial precipitation for the duration of the experiment (1–10 July). The amount of rainfall corresponded to actual irrigation water applied in the field ($\sim$11 mm day^{-1}). This led to complete saturation of soil ($\Theta_i = 0.40$) in the model. To fully simulate irrigation conditions, canopy interception re-evaporation was disabled in the LSM, imitating the furrow irrigation practice common in southeastern Turkey. This forced total water input to evaporate/transpire only through soil and vegetation, but not before reaching the ground surface.

5. Penman-based estimate of potential evaporation

The calibration data used in this study is the same dataset described by Ozdogan and Salvucci (2004) collected at the Harran–Koruklu station (see the star on Fig. 2). We used daily mean values of temperature, radiation, wind speed, soil temperature, and humidity, all measured at the standard 2-m height, to compute E_p, E_w, and E_a based on the CR concepts. In summary, it is based on calibrating the Penman potential evaporation (Penman 1948) to observed pan evaporation by adjusting roughness length Z_0. However, the analysis is further complicated because we have incorporated the effects of atmospheric stability using an estimate of the sensible heat flux.

Penman's widely used equation for potential evapotranspiration for a free water surface combines the energy budget and mass transfer approaches, leading to

$$\lambda E_p = \frac{\varepsilon_{\text{sa}} r_{aH}(R_N - G) + \rho\lambda D_a}{\varepsilon_{\text{sa}} r_{aH} + r_{aE} + r_s}. \tag{4}$$

In (4), λ is the latent heat of vaporization, ρ is the air density, r_{aH} and r_{aE} are the aerodynamic resistance for heat and vapor transfer, r_s is the bulk surface resistance, D_a is humidity deficit at the reference point, R_N is net radiation at the surface, G is ground heat flux, and ε_{sa}

is the slope of saturation specific humidity, linearized around T_a,

$$\varepsilon_{\text{sa}} = \frac{\lambda}{C_p}\left[\frac{dQ_{\text{sat}}}{dT}\right]_{T=T_a}. \quad (5)$$

Mahrt and Ek (1984) note the importance of atmospheric stability on aerodynamic resistance for heat (r_{aH}) and vapor (r_{aE}) transfer in potential evaporation explained by Eq. (4). Accordingly, r_{aH} and r_{aE} were computed by

$$r_{aH,E} = \left[\ln\left(\frac{Z_r}{Z_0}\right) - \psi_{H,E}\right]\frac{1}{ku_*}. \quad (6)$$

In (6), Z_r is the reference height (2 m), Z_0 is the roughness length (seasonally varying; see Fig. 3), k is the von Kármán's constant (0.41), u^* is the friction velocity, and ψ_H and ψ_E are the stability corrections for heat and vapor transfer, respectively, as a function of the Monin–Obukhov length. The details concerning these stability correction factors are well established and can be found in Brutsaert (1982) and Garratt (1992). The values for u_* are obtained from wind speed at reference height (U_2) and roughness length (Z_0) as

$$u_* = \frac{k * U_2}{\ln(Z_r/Z_0) - \psi_M}. \quad (7)$$

In (7), ψ_M is the stability correction for momentum transfer as mentioned above. Note that in this study, the roughness length for heat/moisture and momentum are assumed to be identical in resistance correction terms. Under nonneutral conditions, however, these roughness lengths may differ up to several orders of magnitude as a function of surface temperature over most natural homogeneous surfaces (Brutsaert 1982; Garratt 1992; Stewart et al. 1994, Brutsaert 1999). Nevertheless, given the nature of surface temperature computed as a residual of the surface energy balance [Eq. (8)] as well as the extensive calibration procedure described below, we believe our results are not very sensitive to the exact formulation of these resistances.

To incorporate the above stability effects as would be felt by the meteorological site where the evaporation pan is located, the average sensible heat flux from the Harran Plain was estimated. This large-scale flux is here referred to as the environmental sensible heat flux (H_{ENV}) to distinguish it from the sensible heat flux that would occur from the pan itself (H_{pan}). The critical distinction is that we use H_{ENV} to estimate the stability corrections and not H_{pan}, because the pan is too small to influence the boundary layer. The calibration procedure thus required that two land surface energy balances be computed: one for the environment (SEB_{ENV})

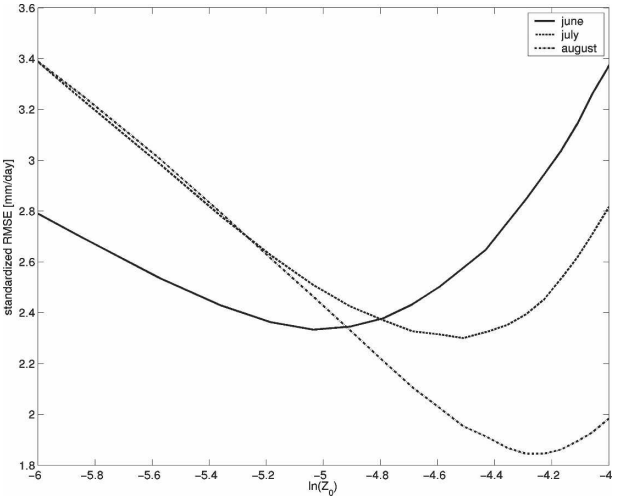

FIG. 3. Standardized rmse between potential and pan evaporation data for different roughness length (Z_0) values for three summer months in the Harran Plain. The data is the 20-yr average for each month.

and another for the meteorological site (meant to represent the evaporating pan) (SEB_{met}). In each SEB, the basic-state variable is the surface temperature (T_s):

$$[R_{\text{SW}\downarrow}(1 - \alpha_s) + e_S(R_{\text{LW}\downarrow} - \sigma {T_{s,\text{pan}}}^4)] - G - E_{\text{pan}} - H_{\text{pan}} = 0, \quad (8)$$

$$[R_{\text{SW}\downarrow}(1 - \alpha_s) + e_S(R_{\text{LW}\downarrow} - \sigma {T_{s,\text{ENV}}}^4)] - G - E_{\text{WB}} - H_{\text{ENV}} = 0. \quad (9)$$

In both of these equations, α_s is surface albedo and e_S is emissivity; $R_{\text{LW}\downarrow}$ was estimated with expression from Brutsaert (1982). Again, the principal goal here was to calculate the ψ terms (via H_{ENV}) to account for the effects of environmental instability on pan evaporation. In Eq. (8), E_{pan} is modeled using a saturated surface humidity (these are the values that are compared with the pan data for estimation of Z_0 in Fig. 3). In Eq. (9), on the other hand, evaporation is set to its observed value from water balance (E_{WB}), allowing H_{ENV} to be estimated as a residual of SEB_{ENV} via G and net radiation [Eq. (9)]. The stability correction factors computed as a function of H_{ENV} are then used within the meteorological site-based energy budget to compute fluxes that corresponded to a unique surface temperature [Eq. (8)]. Note that in order to achieve closure in both SEBs, Eqs. (8) and (9) were solved for $T_{s,\text{pan}}$ and $T_{s,\text{ENV}}$ simultaneously through iteration because of the implicit dependence of sensible heat in u^* (through ψ_M) and in r_{aH} and r_{aE} (through ψ_H and ψ_E). As alluded to in the previous section, the whole process was repeated for a range of Z_0 estimates until the best fit was obtained

between measured pan evaporation and predictions (Fig. 3). Note that pan evaporation is known to exceed potential evaporation because of increased water temperature as well as ventilation. In Eq. (8), the T_{pan} variable—computed as a residual of SEB_{met}—partly accounts for this elevated temperature effect. Additionally, the uncertainty around the surface temperature as well as the nature of the evaporating pan (not raised above the ground surface) at this site suggests less-than-significant ventilation effects. Thus no adjustments were made to the pan evaporation data.

6. Evaluation of the complementary relationship

Evaluation of the CR also involves an estimation of E_w, which is calculated based on the concepts proposed by Priestley and Taylor (1972) for conditions of minimal advection. These concepts have led to the development of an equation for potential evaporation given by

$$\lambda E_w = \alpha \frac{\varepsilon}{\varepsilon + 1}(R_N - G). \quad (10)$$

In (10), the value of the constant α, the well-known Priestley–Taylor parameter, is reported to be 1.26, although it represents the climatological mean. A number of studies have reported that α can range between 1.0 and 1.5 (Lhomme 1997; Kim and Entekhabi 1997; Raupach 2000).

For comparison with CR estimates [Eq. (3)], we used an independent estimate of E_a from Ozdogan et al. (2006) who computed seasonal water use for irrigation in the study area for the period 1980–2001 based on estimates of irrigated acreage from remote sensing. While no actual evaporation measurement was available for validation of computed fluxes, this total seasonal irrigation, expressed as $[LT^{-1}]$, was the best independent water-balance-based estimate of E_a.

In evaluating CR, we (i) analyze the changes in E_p and E_a, simulated by the mesoscale model, for increasing surface moisture conditions; (ii) compare the climate model simulations of E_p and E_a to the computed fluxes from the station data as averaged over the simulation period; (iii) perform sensitivity analyses with the calibrated potential evaporation equation to explore the relative importance of environmental variables for maintaining complementarity; and (iv) explore the larger-scale, dynamical feedbacks controlling wind speed changes.

7. Results and discussion

Previous assessments of the ability of the NCEP Regional Spectral Model to simulate fluxes have been encouraging. For example, Anderson et al. (2000, 2004) show that the RSM can successfully simulate the intraseasonal variations in the climatological summertime hydrologic cycle as well as low-level monsoon winds over the southwestern United States. Brenner (2000) also report good agreement between RSM-simulated and observed surface wind speed in the eastern Mediterranean region. Below, the model results, meteorological data, and recalibrated Penman potential evaporation equation, as well as the CR, are evaluated for the irrigated plains over southeastern Turkey.

a. Complementary relationship within calibrated Penman equation

Figure 4a shows the trend in potential evaporation calculated with the calibrated Penman equation (triangles). There is a strong decreasing trend in E_p, suggesting potential evaporation has been greatly affected by irrigation under nonneutral conditions. The same trend is also visible in pan evaporation data (circles), although it has more scatter. Figure 4b shows the CR concept where computed E_p decreases as actual evaporation (shown as the shaded area) estimated from water balance increases in a complementary fashion. Also plotted in Fig. 4b is the CR-based estimate of actual evaporation (circles). The good fit between the shaded area and this estimate (Table 1) lends credibility to actual evaporation estimation capabilities of the CR,

TABLE 1. Quantitative measures of model performance suggested by Willmott (1982) for predicting latent heat flux* (in W m^{-2}).

N	$\overline{LE}_{model}$	$\overline{LE}_{WB}$	S_{model}	S_{WB}	MAE	Rmse	$Rmse_S$	$Rmse_U$	d	r^2
23	120	112	86	94	30	33	15	29	0.96	0.88

* In the table, $\overline{LE}_{model}$ is mean latent heat flux computed with the model; $\overline{LE}_{WB}$ is mean latent heat flux computed with the water balance method; S_{model} is the standard deviation of latent heat flux computed with the model; S_{WB} is the standard deviation of latent heat flux computed with the water balance method; mean absolute error (MAE) is $N^{-1}\Sigma_{i=1}^{N}|LE_{model,i} - LE_{WB,i}|$; rmse is $[N^{-1}\Sigma_{i=1}^{N}(LE_{model,i} - LE_{WB,i})^2]^{0.5}$; systematic rmse ($rmse_S$) is $[N^{-1}\Sigma_{i=1}^{N}(LE^{\wedge}_{model,i} - LE_{,WB,i})^2]^{0.5}$; unsystematic rmse ($rmse_U$) is $[N^{-1}\Sigma_{i=1}^{N}(LE_{model,i} - LE^{\wedge}_{WB,i})^2]^{0.5}$; $LE^{\wedge}_{model,i} = a + b\,\overline{LE}_{WB,i}$ is predicted model result using linear regression; $d = 1 - [\Sigma_{i=1}^{N}(LE_{model,i} - LE_{WB,i})^2/\Sigma_{i=1}^{N}(|LE'_{model,i}| - |LE'_{WB,i}|)^2]$, where $0 \le d \le 1$ is index of agreement; $LE'_{model,i} = LE_{model,i} - \overline{LE}_{WB}$ and $LE'_{WB,i} = LE_{WB,i} - \overline{LE}_{WB}$; and r^2 is squared correlation coefficient.

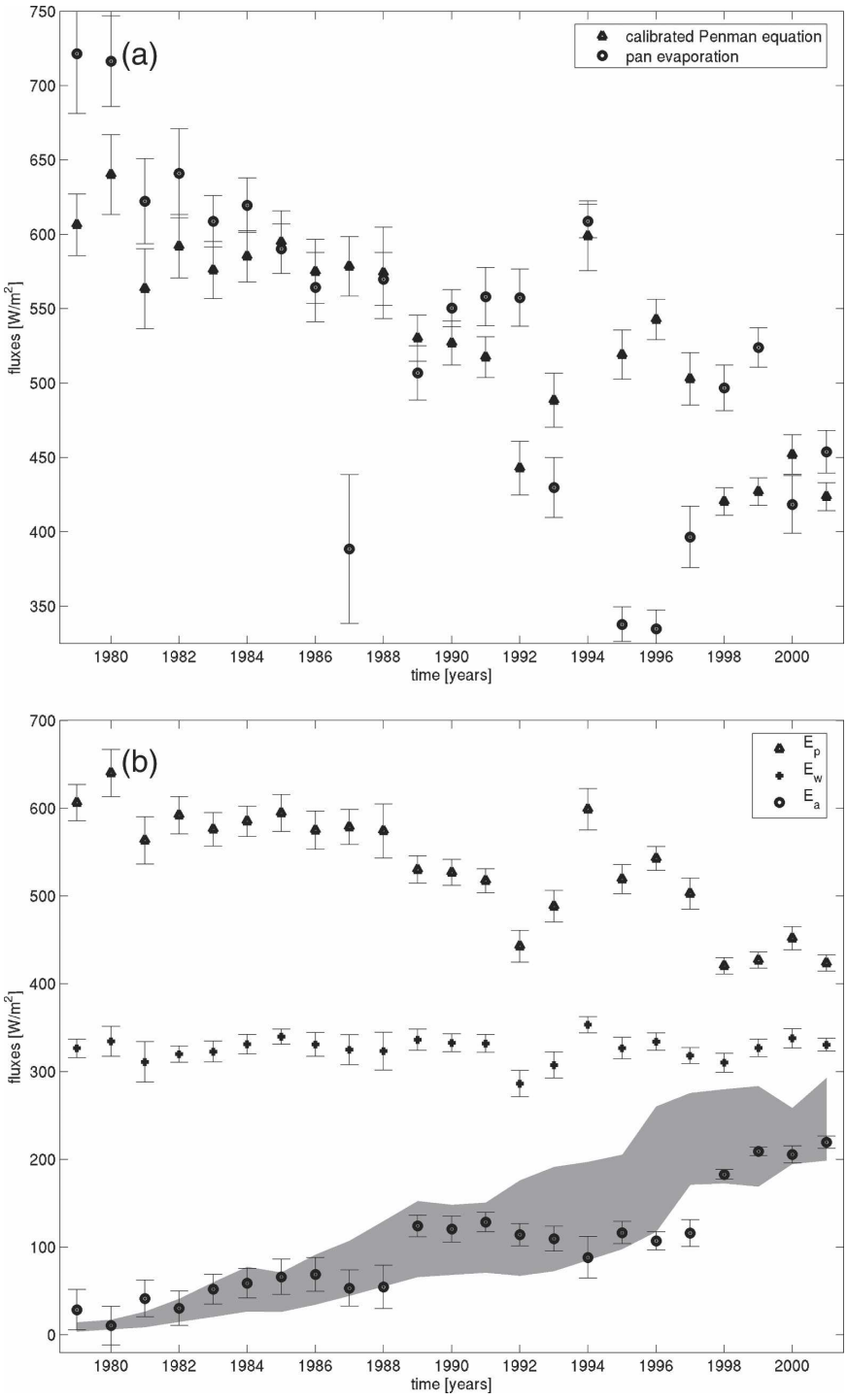

FIG. 4. (a) The relationship between potential evaporation computed with the recalibrated Penman equation and measured pan evaporation data for the Harran Plain. The 90-day average is shown. Error bars represent one standard deviation. (b) Complementary relationship between E_p, E_w, and E_a. The shaded area represents the uncertainty range in water-balance-based E_a estimates derived from irrigation water use. Error bars represent one standard deviation.

making it a useful hydrologic monitoring tool with minimum data requirements. That is, one can compute potential evaporation (or take pan evaporation) and estimate actual evaporation based on the complementary theory [Eq. (3)]. Given the planned large irrigation schemes in southeastern Turkey, the existence of CR provides significant capacity to estimate evaporation over large areas with minimum data requirements.

b. Complementary relationship within the RSM model

Figures 5a and 5b show the potential and actual evaporation, as predicted by the RSM over the Harran Plain, temporally averaged over the simulation period (1–10 July) for 20 irrigation years. Both graphs show the average response of all grids representing the Harran Plain (thick solid line). Here we show the plain average because intuitively, one would expect to observe strong interaction between grid points (through advection) so that the effects of irrigating one (or more) grids would strongly influence fluxes from the neighboring nonirrigated grids. Indeed, our original expectation was that as more and more neighboring grids were irrigated, the potential evaporation from grid 55 (Fig. 2) would decline as a result of the feedback process within the boundary layer. However, once irrigated, grid 55 quickly reached its minimum potential evaporation, and changing environmental conditions further within the PBL—either directly above the irrigated grid or at neighboring grids—had very little impact. The same was also true of other grids that go in and out of irrigation (i.e., as irrigation shifts over 20 yr). This indicates a relative lack of simulated lateral interactions among grids. Presumably, higher-resolution (both horizontally and vertically) models with better-resolved turbulence (e.g., Avissar and Chen 1993; Chen and Avissar 1994) would be required to see the lateral interactions originally expected.

The main point of the graphs shown in Figs. 5a and 5b is to demonstrate that over the entire Harran Plain, both potential (thick black solid line, Fig. 5a) and actual evaporation (thick black solid line, Fig. 5b) respond to increased moisture availability at the surface: potential evaporation decreases with increasing evaporation as hypothesized by the complementary relationship. Furthermore, the ratio of rates of change for E_p and E_a with respect to available soil moisture over time is close to -1, which corresponds to a strict complementarity. This finding lends further simulation-based credibility to the CR, making it a useful hydrologic monitoring tool with minimum data requirements.

Also plotted in Fig. 5a is E_p obtained from the calibrated Penman equation. There is a strong correlation between the observed and spatially averaged modeled data. Here E_p from recalibrated Penman equation (circles) decreases with time at the same rate as its model estimate, going from 650 to about 400 W m^{-2}. Note that there is a large scatter in this estimate, and this scatter can be partially attributed to the averaging window (10 days) over the warm season. The seasonal average (90 days) of computed evaporation (shown in Fig. 4a) shows much less variation.

It should also be noted here that the good fit between simulated and water balance latent heat flux (Fig. 5b) is an expected result. In a semiarid environment like the Harran Plain with large potential for evaporation, most of the water input into the system (e.g., through irrigation) is expected to evaporate. Essentially, if all irrigation is evaporated, then the irrigation itself forms an estimate of the latent heat flux. The fit also implies that the soil-related parameters used in the model are realistic: irrigation is mostly partitioned into evaporation, not drainage.

Two conclusions can be drawn from the correlations in Fig. 5: 1) The adjustment of initial soil moisture conditions and roughness length for the numerical experiment was realistic, and 2) spatially averaged modeled fluxes over the entire Harran Plain are representative of the irrigation-induced processes.

c. Intercomparison of M–O scaling variables

Ozdogan and Salvucci (2004) reported a strong wind speed contribution to the decline in observed in E_p over the Harran Plain, which was partly attributed to increased surface roughness (as evident in Z_0 shown in Fig. 3). This research presents a unique opportunity to study this wind effect of irrigation in more detail. It is logical to first compare modeled wind velocity to observed wind speed at the reference height (2 m). However, this task is not straightforward. First, the model context significantly differs from the real world due to bulk parameterization of surface elements. For example, as described in the roughness length discussion above, the average roughness length used in the model is 0.5 m for the entire domain. Using standard rules of thumb, this corresponds roughly to 4-m-high surface elements (topography, trees, crops, bushes, etc.), which may be unrealistic but useful in the context of a model, where the lateral resolution is ~10 km. Thus, in order to compare variables that change with height such as wind speed, humidity, and temperature, an appropriate scaling procedure is needed. The solution proposed here is to use the scaling parameters of the M–O similarity profiles: u^* (friction velocity) for U (wind speed); q^* (humidity scale) in place of q (specific humidity); and Θ^* (temperature scale) for T (temperature). Brut-

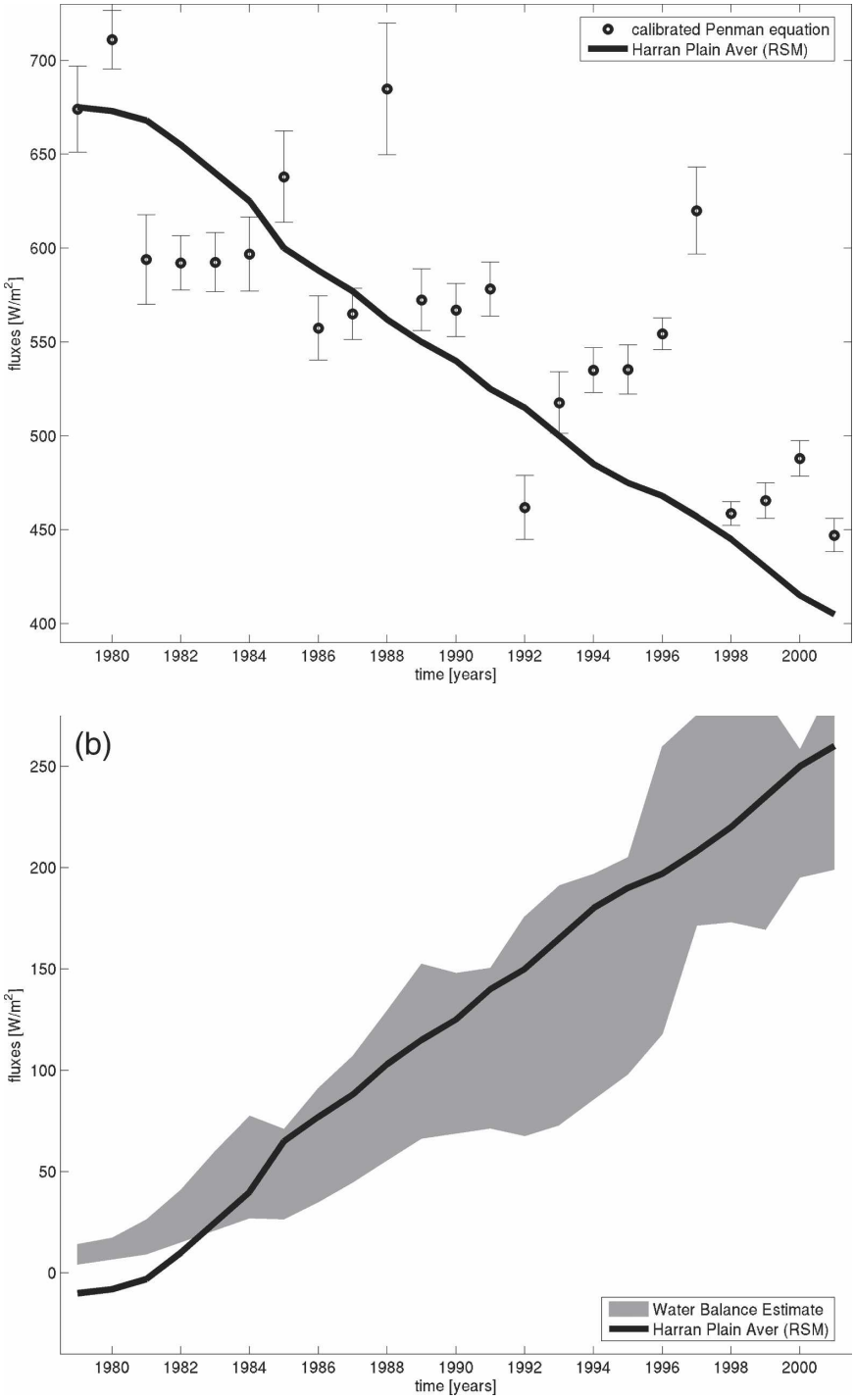

FIG. 5. (a) Warm season potential evaporation predicted by the RSM climate model (solid line) and calculated with the observed quantities from the meteorological station (circles) the Harran Plain. Simulated (RSM) potential evaporation was derived by the Land Surface Model using a Penman-type approach. Error bars on the observed quantities represent one standard deviation. (b) Warm season actual evaporation in the Harran Plain predicted by the RSM climate model (solid line). Also shown are observed quantities from water balance (shaded area). Simulated (RSM) actual evaporation was predicted using standard surface flux calculations by the Land Surface Model. The shaded area represents the uncertainty range in the water balance estimate.

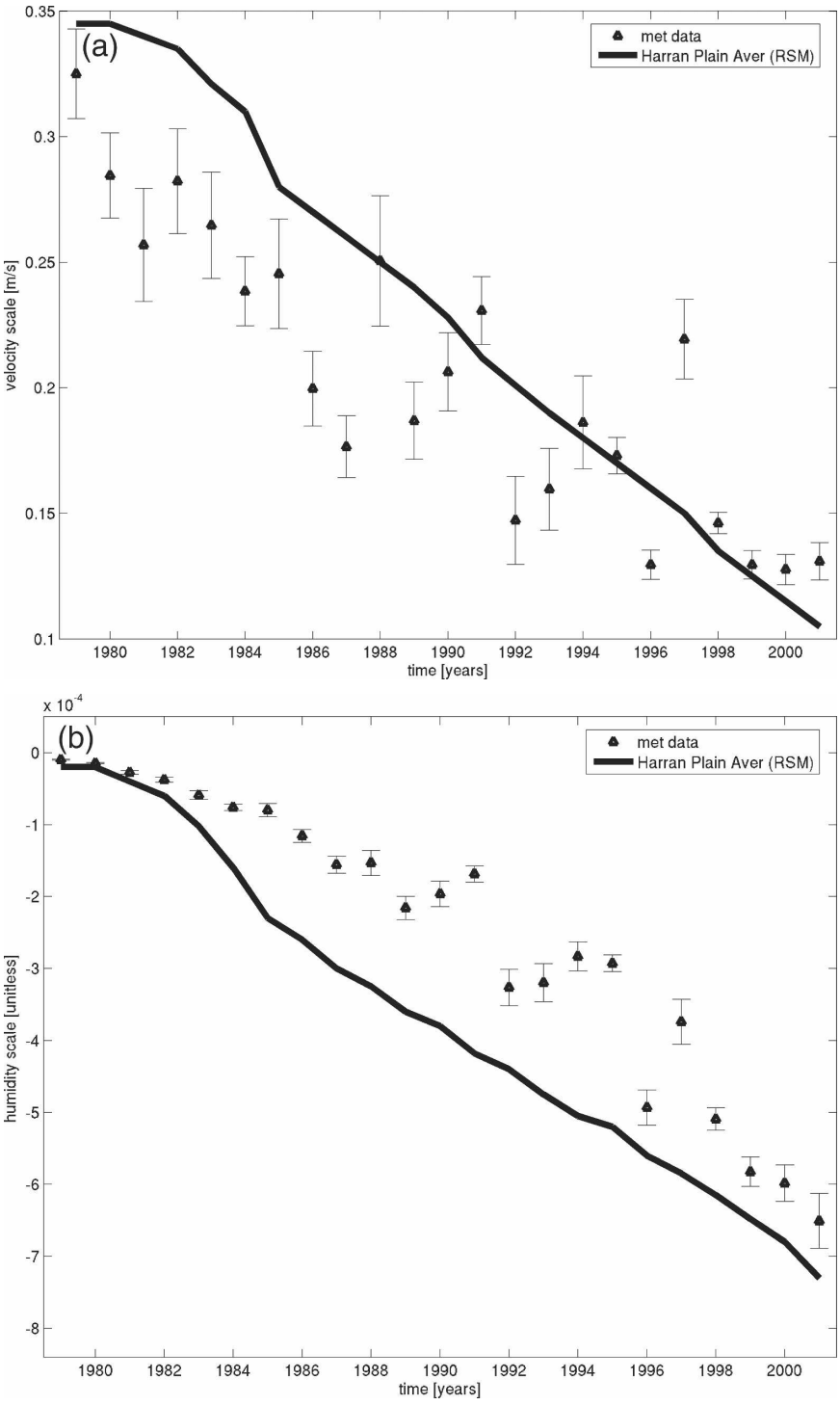

FIG. 6. (a) Observed (triangles) and RSM-simulated (solid black line) velocity scale (u^*) in the Harran Plain. Simulated (RSM) velocity scale was computed using a prescribed profile with similarity-based scale parameters. Error bars on the observed quantities represent one standard deviation. (b) Observed (triangles) and RSM-simulated (solid black line) humidity scale (q^*) in the Harran plain. Simulated (RSM) humidity scale was computed using a prescribed profile with similarity-based scale parameters. Error bars on the observed quantities represent one standard deviation. (c) Observed (triangles) and RSM-simulated (solid black line) temperature scale (Θ^*) in the Harran Plain. Simulated (RSM) temperature scale was computed using a prescribed profile with similarity-based scale parameters. Error bars on the observed quantities represent one standard deviation.

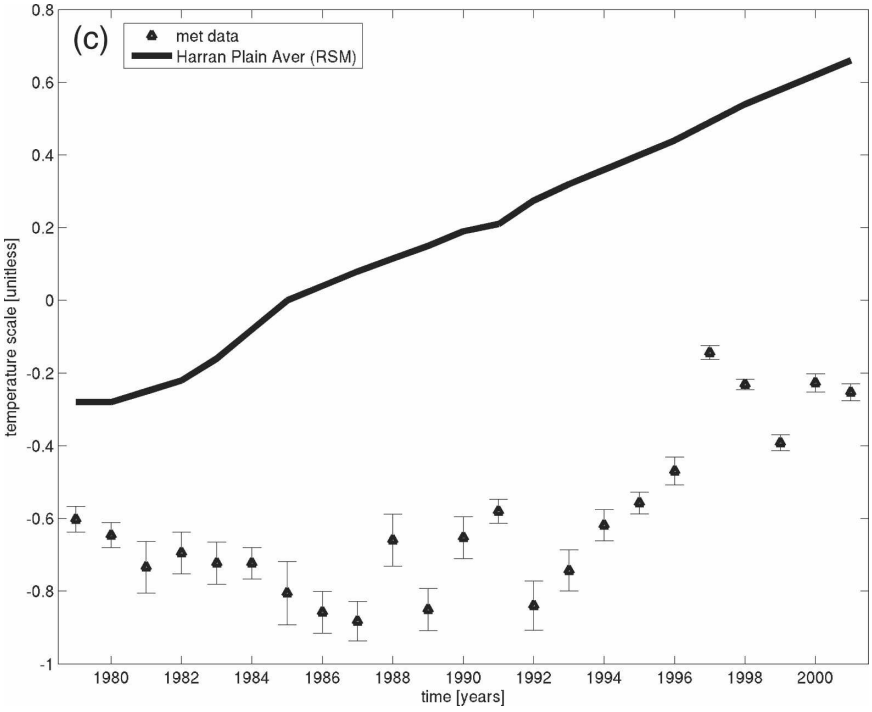

FIG. 6. (*Continued*)

saert (1982) and Garratt (1992) provide appropriate expressions for profile-based and the flux-based estimates of these quantities.

Figures 6a–c show the relationship between modeled and observed scaling parameters of the M–O similarity hypothesis as a function of irrigation over the Harran Plain. The time series velocity scale (u^*) between the model and observations agree considerably, suggesting that both modeled and observed quantities describe a similar magnitude of changes in wind speed. On the other hand, the humidity scale (q^*) shows less agreement, indicating that the sensitivity of the model grid and meteorological station to irrigation are different. Nevertheless, these results have important implications for evaluating CR. For example, decreased mixing in the PBL and, to a lesser degree, depressed humidity deficit as a function of irrigation are the primary causes of decreased E_p.

Another conclusion that can be drawn from this measurement/model agreement is that the comparison between modeled and observed variables is best achieved when the absolute heights of measurement and model level are taken out of the process via profile scaling. This is particularly useful in cases where the vertical scales of actual and modeled roughness elements differ considerably due to the lateral resolution of the model. In such cases, the roughness heights used in the model will be larger (to include subgrid topographic roughness effects). For example, when specific humidity data are compared at the same absolute height (2 m), their sensitivity to irrigation is not as pronounced as their scaled equivalents. The results obtained from these two analyses thus provide a procedure on how to compare model results to observations, especially for variables that change with height.

While the relative temperature change is similar, there is a bias between the model estimate of the temperature scale (Θ^*) and its estimate from field data. This difference stems mainly from the difference in sensible heat flux, which in turn is a function of available energy. The formulation of available energy (downwelling and upwelling radiation as well as ground heat flux) is different between the RSM model and validation dataset, showing a $\sim$150 W m^{-2} bias. This difference is mostly due to different albedo and emissivity treatments of the surface [see Ozdogan (2005) for further discussion].

d. Mechanisms for the complementary relationship

The good correlations between modeled and observed fluxes and the height-independent M–O similarity parameters also provide an opportunity to learn more about the mechanisms that maintain complementarity between potential and actual evaporation. To do this, the Penman equation [Eq. (16)] was rewritten to emphasize the dependence on stability effects:

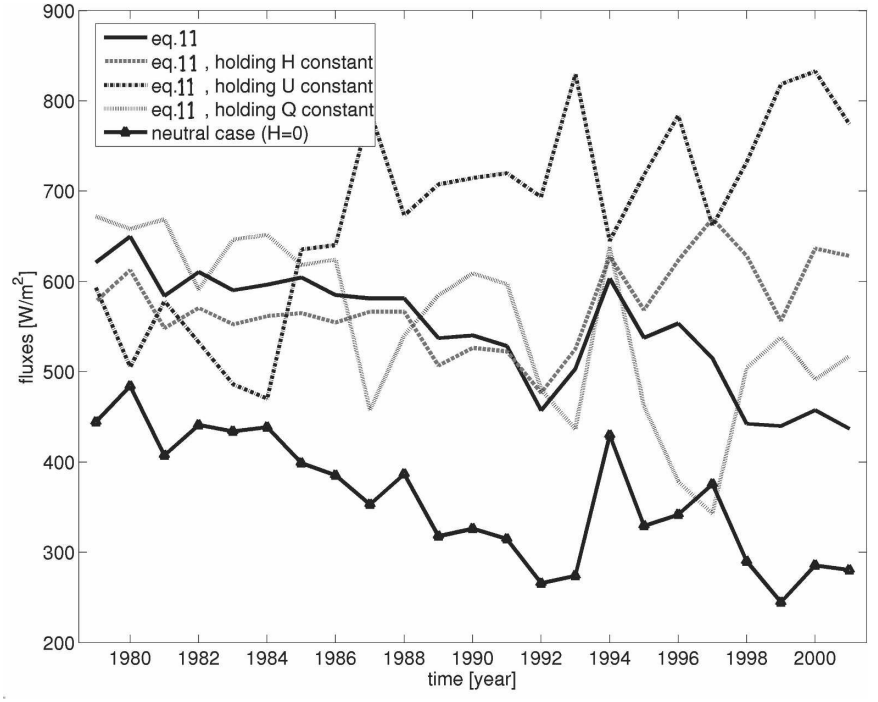

FIG. 7. Sensitivity of potential evaporation to different input parameters estimated by holding one variable constant at a time within Eq. (11). "Neutral case" is when stability effects have been removed. See text for details.

$$E_p\lambda = \frac{\varepsilon_{sa} r_{aH}(z, Z_0, [U[H_{ENV}]]) \, (R_N - G) + \rho\lambda D_a(q_a)}{\varepsilon_{sa} r_{aH}(z, Z_0, [U[H_{ENV}]]) + r_{aE}(z, Z_0, [U[H_{ENV}]]) + r_s}. \quad (11)$$

By holding each of the variables in Eq. (11) constant while allowing the others to vary over the 23-yr course of irrigation, the influence of increased evaporation on E_p, as heuristically explained by the CR, can be explored in greater detail (Fig. 7).

Results indicate that both wind speed and stability effects are important in maintaining complementarity. For example, when the effects of wind speed are limited by holding the wind speed constant at its mean value, potential evaporation increases slightly with increasing evaporation (dashed black line, Fig. 7), indicating that the decrease in wind speed with irrigation plays a primary role in producing a decrease in potential evaporation. Note that this decrease is not in and of itself enough to reduce actual evaporation, which increases due to increases in the overlying land/atmosphere moisture gradient. Similarly, if sensible heat flux is held constant at its mean ($\sim$130 W m^{-2}), then atmospheric stability will remain constant and potential evaporation is higher than in the control estimate, especially for higher irrigation years (dashed gray line, Fig. 7). This lack of increase in stability counteracts the decreasing effect of wind speed, leading to a neutral/slightly increasing trend in potential evaporation over time. Only when the effects of both stability and wind speed are simultaneously in operation does potential evaporation show a decreasing trend, indicating that dynamical effects are an important part of the complementary theory. The effects of decreasing humidity deficit appear to be also important (light gray line, Fig. 7), but in southeastern Turkey, dynamics are more important for maintaining CR.

e. Possible explanations for wind speed decrease

In general, the relationship between potential and actual evapotranspiration, as described by the CR, has been defined based solely on the degree to which soil/vegetation continuum can satisfy the atmospheric water vapor demand and consequent changes in energy partitioning at the land–atmosphere interface (e.g., Kim and Entekhabi 1997; Szilagyi 2001). The changes in this relationship due to dynamical effects such as wind speed in the presence of irrigation are an unexpected finding of this research and merit further discussion.

Two plausible explanations are considered here for the observed decrease in wind speed. The first irriga-

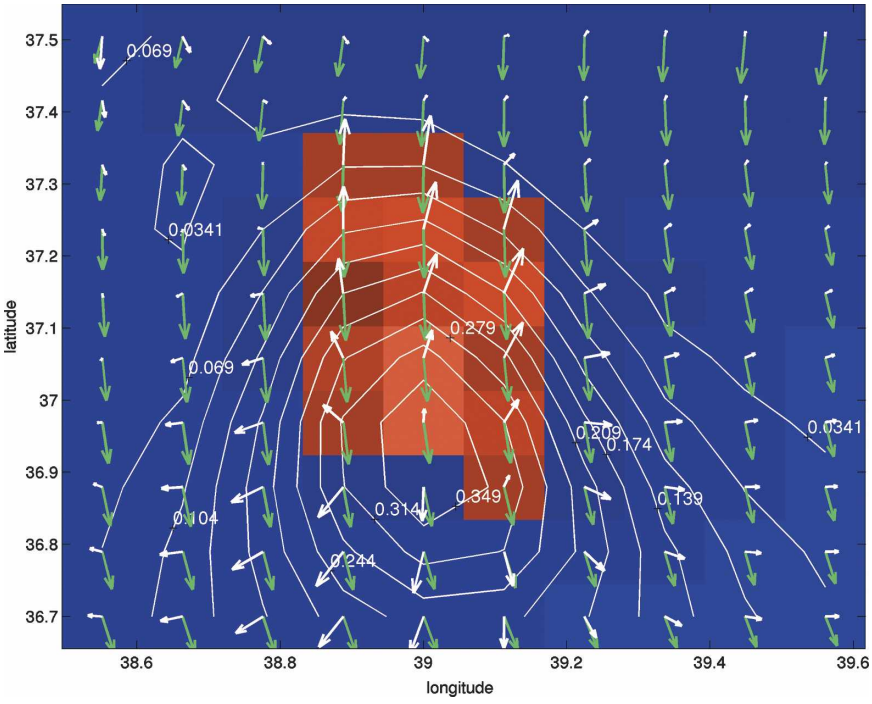

FIG. 8. Simulated surface (2 m) wind fields. The contour lines plot the difference in surface pressure before and after irrigation (hPa). Green arrows represent background flow before irrigation. White arrows represent the difference in wind field after irrigation minus wind field before irrigation. Over the Harran Plain (shown in red), locally generated winds counteract the background flow. Note that the white arrows have been exaggerated (2 ×) to show effect. The figure shows a 10 × 10 window of the large simulation domain.

tion-related factor is related to surface roughness. Vegetated surfaces generally add to aerodynamic surface roughness, which, in turn, has the potential to slow down near-surface wind velocities through the increases in friction between the low-level atmosphere and surface (Burman et al. 1975; Alpert and Mandel 1986).

The second is related directly to soil moisture. A number of field experiments as well as modeling studies on the near-surface meteorological effects of inhomogeneous surface moisture characteristics have shown evidence of locally generated wind systems arising from differential heating of adjacent areas such as irrigated patches among dry natural vegetation (Segal et al. 1989; Segal and Arritt 1992; Doran et al. 1995; De Ritter and Gallee 1998). Often referred to as "nonclassical mesoscale circulations," these wind systems are caused by strong thermal and pressure gradients over the interface between wet (irrigated) and dry surfaces, similar to that of sea-breeze formation. The locally generated flow due to these adverse gradients (i.e., higher pressure over cool irrigated areas) has the potential to counteract the main flow regime and decelerate the background wind velocity (Segal et al. 1989; Doran et al. 1995). This hypothesis was evaluated by comparing the difference in individual vector components of wind speed over the Harran Plain before (control run) and after (year 16) irrigation (Fig. 8). Since all background climatic conditions are held constant, the difference wind field is solely due to irrigation. Also shown here is the difference in surface pressure centered over the irrigated grids before and after irrigation. Most of the difference vectors follow the pressure difference gradient and are in the opposite direction of the background (nonirrigated) flow.

The comparison presented above provides evidence for the existence of locally generated wind systems, originally suggested by Segal et al. (1989). However, as described above, the irrigation experiments also include a roughness factor. To separate the drag effects on wind caused by increased roughness at the surface from the nonclassical mesoscale circulations that also affect wind speed, results from additional "smooth" experiments, where roughness was not changed for irrigated grids, were compared to "rough" experiments described in section 4. Comparison of the results from the rough/irrigated experiment to those obtained from the smooth/irrigated experiment reveals roughness-related

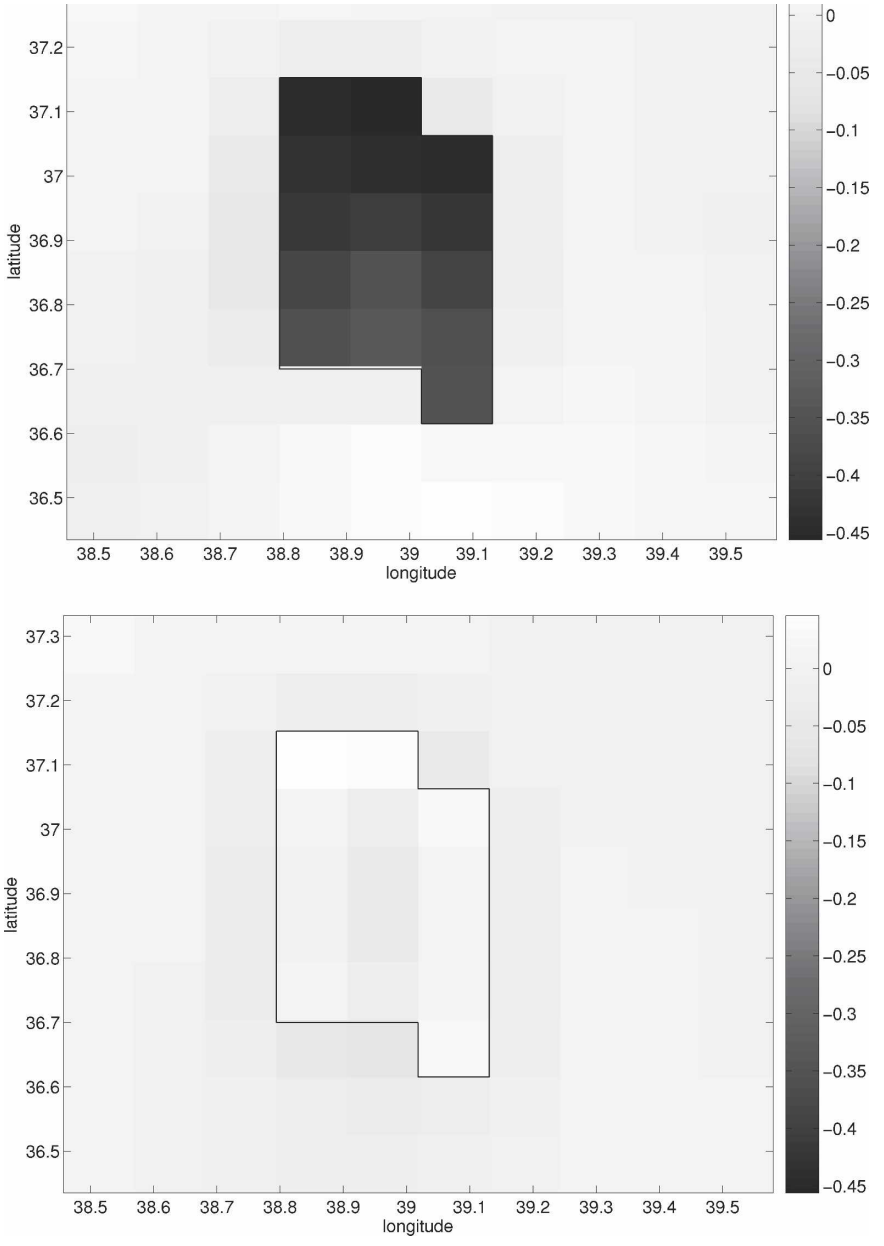

FIG. 9. Spatial pattern of changes in friction velocity (top) due to both irrigation and roughness and (bottom) due only to roughness. These results were obtained by subtracting nonirrigated smooth run results from nonirrigated rough run. The units are in m s^{-1}.

effects. Similarly, comparison of a rough/nonirrigated experiment to a rough/irrigated experiment provides information on only the irrigation component. The results are given in Figs. 9a and 9b in terms of the velocity scale u*. As shown, roughness accounts for only about 1% of the decrease in friction velocity while irrigation accounts for the almost all of the observed decrease, indicating the significance of irrigation.

Irrigation, when practiced over relatively large length scales ($>$ 5 km), also has the potential to decrease convectively driven turbulence that partially ventilates the lower atmosphere. Irrigated lands are characterized by high rates of evaporation accompanied by little transfer of sensible heat flux. This reduction in sensible heat transfer leads to a partial collapse of convectively driven turbulence that inhibits mixed-layer growth and increases the stability of near-surface atmosphere. These two effects are shown in Fig. 10 where changes in mixed-layer height and low-level atmospheric stability are plotted as a function of irrigation year. Here the

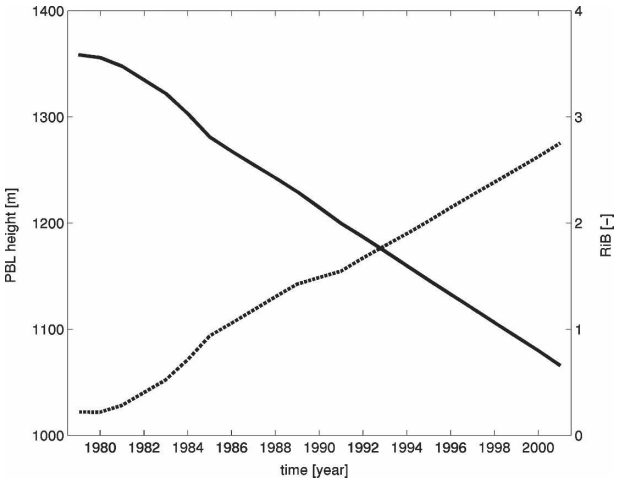

FIG. 10. Simulated changes in mixed-layer height (solid line) and low-level atmospheric stability (dashed line) (represented by bulk Richardson number) as a function of time (irrigation).

near-surface atmospheric stability is represented by the bulk Richardson number (Ri_B) (Arya 2001):

$$\mathrm{Ri}_B = \frac{g}{T_v}\frac{\Delta\theta\Delta z}{(\Delta U)^2}. \tag{12}$$

In (12), T_v is surface virtual temperature, $\Delta\Theta$ is virtual potential temperature difference between two heights represented by (Δz), and ΔU is changes in horizontal wind velocity. As expected, the mixed-layer height is reduced while stability is increased with irrigation. One effect of this increased stability associated with smaller turbulent intensity is to reduce effective atmospheric roughness. While wind gustiness may be negatively influenced under increasingly stable conditions in what is now a smoother lower atmosphere, surface wind speed would be expected to increase. Unfortunately, this effect—in terms of negative contribution to the decrease in friction velocity—cannot be separated from the impact of nonclassical circulations with the current form of the RSM model. However, since this effect would increase wind speed, it implies that the reported decrease in wind speed (Figs. 8 and 9) represents a lower limit of the impact of roughness and nonclassical circulation. In other words, if the atmospheric stability effects could be separated from the thermal circulation/surface roughness effects (e.g., via higher-resolution models) removed from the wind speed signal, one would expect to see a greater decrease in wind speed.

8. Conclusions

The present study was designed to evaluate the complementary relationship between potential and actual evaporation using a mesoscale climate model as well as meteorological data. The gradual expansion of irrigated land area in southeastern Turkey forms the natural setting for such a task. The results indicate that model-simulated potential evaporation decreases as a function of increased irrigated land area and that this decrease is at the same rate as the actual evaporation increase, lending support to the complementary relationship. Given appropriate representations for potential and wet-environment evapotranspiration—for example, through observed pan evaporation or other empirical methods suggested by Brutsaert and Stricker (1979) it becomes a simple matter to compute actual evapotranspiration from routine meteorological observations under complementarity theory. The simulated fluxes of potential evaporation also agree well with the re-estimated potential evaporation equation that includes M–O stability corrections, and with the measured pan evaporation data. Such agreement, in turn, leads to confidence to using the RSM model as a numerical laboratory for studying the meteorological feedbacks (e.g., wind speed decreases with nonclassical mesoscale circulations).

Research using this model output also presents a unique opportunity to find physically meaningful explanations for the CR. The importance of dynamic feedbacks is one such finding. According to the model results, irrigation causes increased surface pressure, which generates localized pressure gradients across which the air flows. This locally generated flow of air is generally in the opposite direction of background wind field. This "counterflow" leads to a decrease in wind speed over irrigated areas, which acts to reduce potential evaporation.

Another effect is thermodynamic in origin and is related to the atmospheric stability. Irrigation, when practiced extensively, increases latent heat flux at the expense of sensible heat flux and this influences the stability of the atmosphere. The resulting increasingly stable conditions reduce mixing in the lower atmosphere (similar to creating a smoother surface), thus further lowering potential evaporation. With stability effects included, potential evaporation calculated over an area is smaller than what it otherwise would be.

Results of this study also lend credibility to the evaporation prediction skill of the RSM model. The model, which forecasts regional meteorological conditions and soil moisture, accurately captures the feedbacks between E_a and E_p even without the use of a detailed land surface/biota component, making it a reasonable forecasting tool for this region.

As stated above, one of the goals here was to find a physical explanation for the CR, for example, through a

conservation principle. However, the results from climate simulations and meteorological data used in a coupled SEB/calibrated Penman equation indicate that the complementarity arises from a combination of mechanisms including feedbacks from dynamics (through wind speed), atmospheric stability (through sensible heat flux), and humidity. This is contrary to some of the earlier work, which suggested the feedbacks from humidity are the only necessary explanation for the complementary relationship (e.g., Szilagyi 2001). The unexpected—and previously unreported—findings of this research related to the feedbacks on partitioning of water between surface and the atmosphere are exciting and form the basis for future research in further evaluating the complementary relation in southeastern Turkey and elsewhere.

REFERENCES

Alpert, P., and M. Mandel, 1986: Wind variability—An indicator for a mesoclimatic change in Israel. *J. Climate Appl. Meteor.,* **25,** 1568–1576.

Anderson, B. T., J. O. Roads, S.-C. Chen, and H.-M. H. Juang, 2000: Regional simulation of the low-level monsoon winds over the Gulf of California and southwestern United States. *J. Geophys. Res.,* **105** (D14), 17 955–17 969.

——, H. Kanamaru, and J. Roads, 2004: The summertime atmospheric hydrologic cycle over the southwestern United States. *J. Hydrometeor.,* **5,** 679–692.

Arya, S. P., 2001: *Introduction to Micrometeorology.* 2d ed. Academic Press, 420 pp.

Avissar, R., and F. Chen, 1993: Development and analysis of prognostic equations for mesoscale kinetic energy and mesoscale (subgrid-scale) fluxes for large-scale atmospheric models. *J. Atmos. Sci.,* **50,** 3751–3774.

Bouchet, R. J., 1963: Evapotranspiration reelle et potentielle, signification climatique. *Proc. IASH General Assembly,* Vol. 62, International Association of Science and Hydrology, 134–142.

Brenner, S., 2000: Wintertime performance of the RSM over the eastern Mediterranean region. *Proc. Second Int. Regional Spectral Model Workshop,* Maui, HI, Scripps ECPC and NCEP, 17–21.

Brutsaert, W., 1982: *Evaporation into the Atmosphere.* D. Reidel, 299 pp.

——, 1999: Aspects of bulk atmospheric boundary layer similarity under free-convective conditions. *Rev. Geophys.,* **37,** 439–451.

——, and H. Stricker, 1979: An advection-aridity approach to estimate actual regional evaporation. *Water Resour. Res.,* **15,** 443–450.

Burman, R. D., J. L. Wright, and M. E. Jensen, 1975: Changes in climate and estimated evaporation across a large irrigated area in Idaho. *Trans. ASAE,* **18,** 1089–1093.

Chen, F., and R. Avissar, 1994: The impact of land-surface wetness heterogeneity on mesoscale heat fluxes. *J. Appl. Meteor.,* **33,** 1323–1340.

——, and Coauthors, 1996: Modeling of land surface evaporation by four schemes and comparison with FIFE observations. *J. Geophys. Res.,* **101,** 7251–7268.

De Ritter, K., and H. Gallee, 1998: Land surface–induced regional climate change in southern Israel. *J. Appl. Meteor.,* **37,** 1470–1485.

Doran, J. C., W. J. Shaw, and J. M. Hubbe, 1995: Boundary layer characteristics over areas of inhomogeneous surface fluxes. *J. Appl. Meteor.,* **34,** 559–579.

Entekhabi, D., and Coauthors, 1999: An agenda for land surface hydrology research and a call for the second international hydrologic decade. *Bull. Amer. Meteor. Soc.,* **80,** 2043–2058.

Garratt, J. R., 1992: *The Atmospheric Boundary Layer.* Cambridge University Press, 316 pp.

Hobbins, M. T., J. A. Ramirez, T. C. Brown, and L. H. J. M. Claessens, 2001: The complementary relationship in the estimation of regional evapotranspiration: The CRAE and Advection–Aridity models. *Water Resour. Res.,* **37,** 1367–1387.

——, ——, and ——, 2004: Trends in pan evaporation and actual evapotranspiration across the conterminous U.S.: Paradoxical or complementary? *Geophys. Res. Lett.,* **31,** L13503, doi:10.1029/2004GL019846.

Hong, S.-Y., and H.-L. Pan, 1996: Nonlocal boundary layer vertical diffusion in a medium-range forecast model. *Mon. Wea. Rev.,* **124,** 2322–2339.

Juang, H.-M. H., and M. Kanamitsu, 1994: The NMC nested regional spectral model. *Mon. Wea. Rev.,* **122,** 3–26.

——, S.-Y. Hong, and M. Kanamitsu, 1997: The NCEP regional spectral model: An update. *Bull. Amer. Meteor. Soc.,* **78,** 2125–2143.

Kalnay, E., and Coauthors, 1996: The NCEP/NCAR 40-Year Reanalysis Project. *Bull. Amer. Meteor. Soc.,* **77,** 437–471.

Kim, C. P., and D. Entekhabi, 1997: Examination of two methods for estimating regional evaporation using a coupled mixed layer and land surface model. *Water Resour. Res.,* **33,** 2109–2116.

Lhomme, J. P., 1997: A theoretical basis for the Priestley–Taylor coefficient. *Bound.-Layer Meteor.,* **82,** 179–191.

Mahrt, L., and M. Ek, 1984: The influence of atmospheric stability on potential evaporation. *J. Climate Appl. Meteor.,* **23,** 222–234.

McNaughton, K. G., and T. W. Spriggs, 1989: An evaluation of the Priestley and Taylor equation and the complementary relationship using results from a mixed layer model of the convective boundary layer. *Estimation of Areal Evapotranspiration,* T. A. Black et al., Eds., International Association of Hydrological Sciences, 89–104.

Monin, A. S., and A. M. Obukhov, 1954: Basic laws of turbulent mixing in the ground layer of the atmosphere (in Russian). *Tr. Geofiz. Inst., Akad. Nauk SSSR,* **24,** 163–187.

Morton, F. I., 1965: Potential evaporation and river basin evaporation. *ASCE J. Hydraul. Div.,* **102** (HY3), 275–291.

Ozdogan, M., 2005: The hydroclimatologic effects of irrigation in southeastern Turkey. Ph.D. dissertation, Boston University, 168 pp.

——, and G. D. Salvucci, 2004: Irrigation-induced changes in potential evapotranspiration in southeastern Turkey: Test and application of Bouchet's complementary hypothesis. *Water Resour. Res.,* **40,** W04301, doi:10.1029/2003WR002822.

——, C. E. Woodcock, G. D. Salvucci, and H. Demir, 2006: Changes in summer irrigated crop area and water use in southeastern Turkey from 1993–2002: Implications for current and future water resources. *Water Resour. Manage.,* in press.

Parlange, M. B., and G. G. Katul, 1992: Estimation of the diurnal

variation of potential evaporation from a wet bare soil surface. *J. Hydrol.,* **132,** 71–89.

Penman, H. L., 1948: Natural evaporation from open water, bare soil and grass. *Proc. Roy. Soc. London.,* **193A,** 120–146.

Priestley, C. H. B., and R. J. Taylor, 1972: On the assessment of surface heat flux and evaporation using large-scale parameters. *Mon. Wea. Rev.,* **100,** 81–92.

Qualls, R. J., and H. Gultekin, 1997: Influence of components of the advection–aridity approach on evapotranspiration estimation. *J. Hydrol.,* **199,** 3–12.

Raupach, M. R., 2000: Equilibrium evaporation and the convective boundary layer. *Bound.-Layer Meteor.,* **96,** 107–141.

Segal, M., and R. W. Arritt, 1992: Nonclassical mesoscale circulations caused by surface sensible heat-flux gradients. *Bull. Amer. Meteor. Soc.,* **73,** 1593–1604.

——, W. E. Schreiber, G. Kallos, J. R. Garratt, A. Rodi, J. Weaver, and R. A. Pielke, 1989: The impact of crop area in northeast Colorado on midsummer mesoscale thermal circulations. *Mon. Wea. Rev.,* **117,** 809–825.

Stewart, J. B., W. P. Kustas, K. S. Humes, W. D. Nichols, M. S. Moran, and H. A. R. deBruin, 1994: Sensible heat flux–radiometric surface temperature relationship for eight semiarid areas. *J. Appl. Meteor.,* **33,** 1110–1117.

Sugita, M., J. Usui, I. Tamagawa, and I. Kaihotsu, 2001: Complementary relationship with a convective boundary layer model to estimate regional evaporation. *Water Resour. Res.,* **37,** 353–365.

Szilagyi, J., 2001: On Bouchet's complementary hypothesis. *J. Hydrol.,* **246,** 155–158.

Willmott, C. J., 1982: Comments on the evaluation of model performance. *Bull. Amer. Meteor. Soc.,* **63,** 1309–1313.